Supplemental Material for "Functional deficits induced by cortical microinfarcts" by Philipp M. Summers, David A. Hartmann, Edward S. Hui, Xingju Nie, Rachael L. Deardorff, Emilie T. McKinnon, Joseph A. Helpern, Jens H. Jensen and Andy Y. Shih

Supplementary Figure 1. Sensory-evoked hemodynamics under awake versus isoflurane-anesthetized conditions. (a) Vibrissae stimulation with air puffs (10 s stimulation, 20 ms air puffs at 8 Hz) results in a marked increase in arteriole diameter when animals are awake, *i.e.,* 0% isoflurane flowing through air in the nose cone. The red line shows average fold change from baseline diameter over time. Error range is standard deviation (n = 9 vessels from 2 animals). **(b)** The same arterioles were re-examined after the mice were anesthetized and maintained under 0.5 % MAC isoflurane in air. **(c,d)** Stimulation-induced diameter changes during control air puffs delivered to the tail, in awake and isoflurane anesthetized states. **(e)** The arteriole diameter at baseline (non-stimulated, no animal activity) was significantly larger during isoflurane anesthesia compared to the awake state ($p = 0.04$, paired t-test; n = 9 arterioles from 2 mice, *i.e.* red dots for mouse 1 and black dots for mouse 2). Data = mean ± SEM. **(f,g)** Awake animals show a larger maximal change in arteriole diameter (panel f) and mean change in arteriole diameter (panel g) compared to during isoflurane anesthesia ($p < 0.005$, paired t-test). **(h,i)** Maximal arteriole diameter (panel h) change to tail puff was not significantly different between awake and isoflurane-anesthetized states ($p = 0.28$, paired t-test). Mean diameter change (panel i) in response to tail puff decreased during isoflurane anesthesia compared to the awake state ($p < 0.002$, paired t-test).

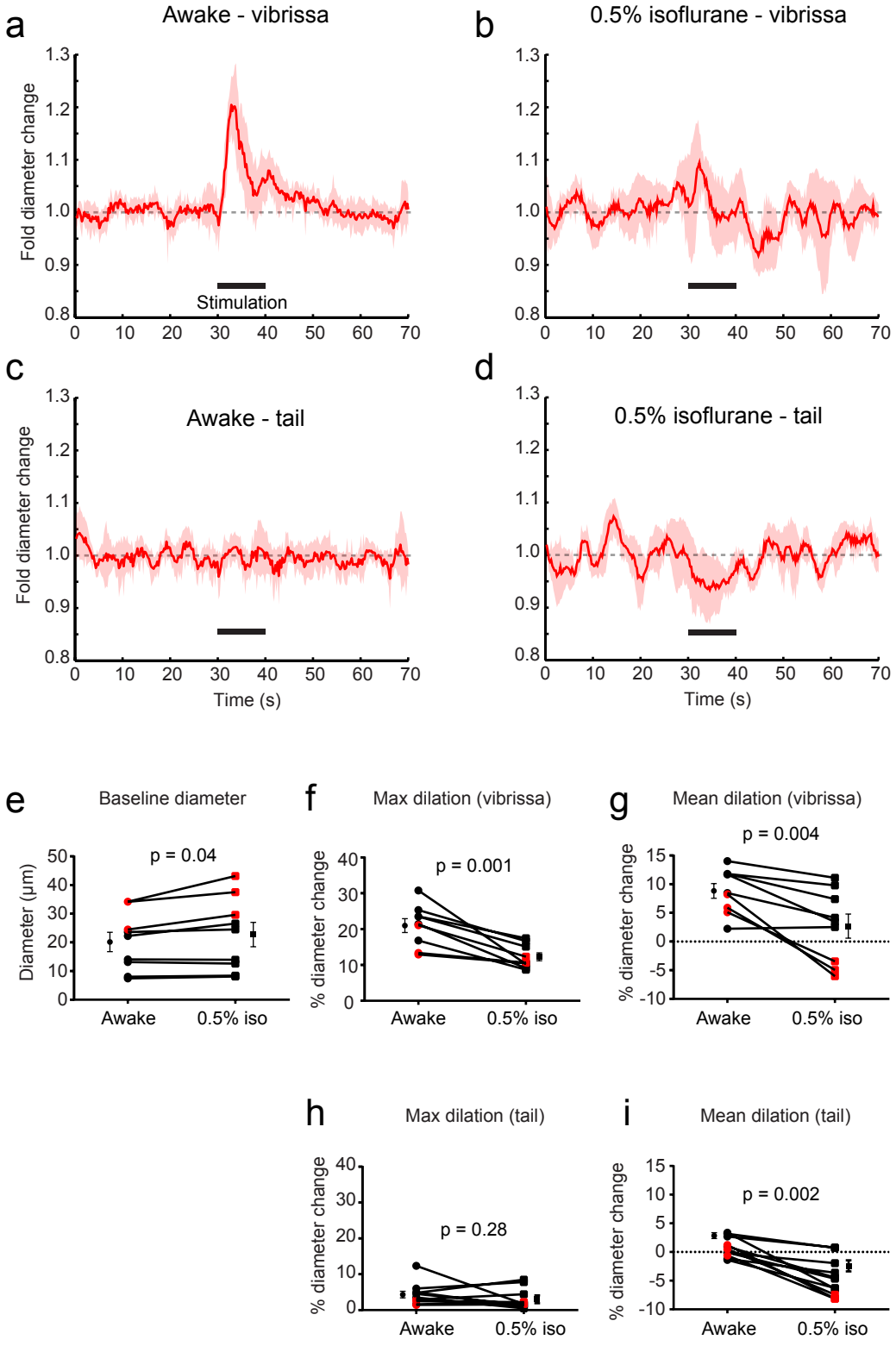

Supplementary Figure 1 (Summers ... Shih)

Supplemental Material for "Functional deficits induced by cortical microinfarcts" by Philipp M. Summers, David A. Hartmann, Edward S. Hui, Xingju Nie, Rachael L. Deardorff, Emilie T. McKinnon, Joseph A. Helpern, Jens H. Jensen and Andy Y. Shih

Supplementary Figure 2. Assessment of sensory-evoked neural activity by *post-mortem* detection of c-Fos protein expression. (a, b) Prolonged stimulation of the whiskers using repeated air puffs (8 Hz, 10 ms pulse duration, 20-minute pulse train) resulted in heightened expression of the immediate early gene, c-Fos, in layer 4 neurons of the contralateral primary barrel cortex (*$p = 0.023$, $t(2) = 6.48$; two-tailed paired t-test; n = 3 mice). **(c, d)** In the same 3 mice, no change was seen with NeuN-positive cell count ($p = 0.83$, $t(2) = 0.24$; two-tailed paired t-test) or VGlut2 intensity ($p = 0.64$, $t(2) = 0.54$; two-tailed paired t-test) for the same mice. Staining for VGlut2 allows for identification of individual barrel locations. Data = mean ± SEM.

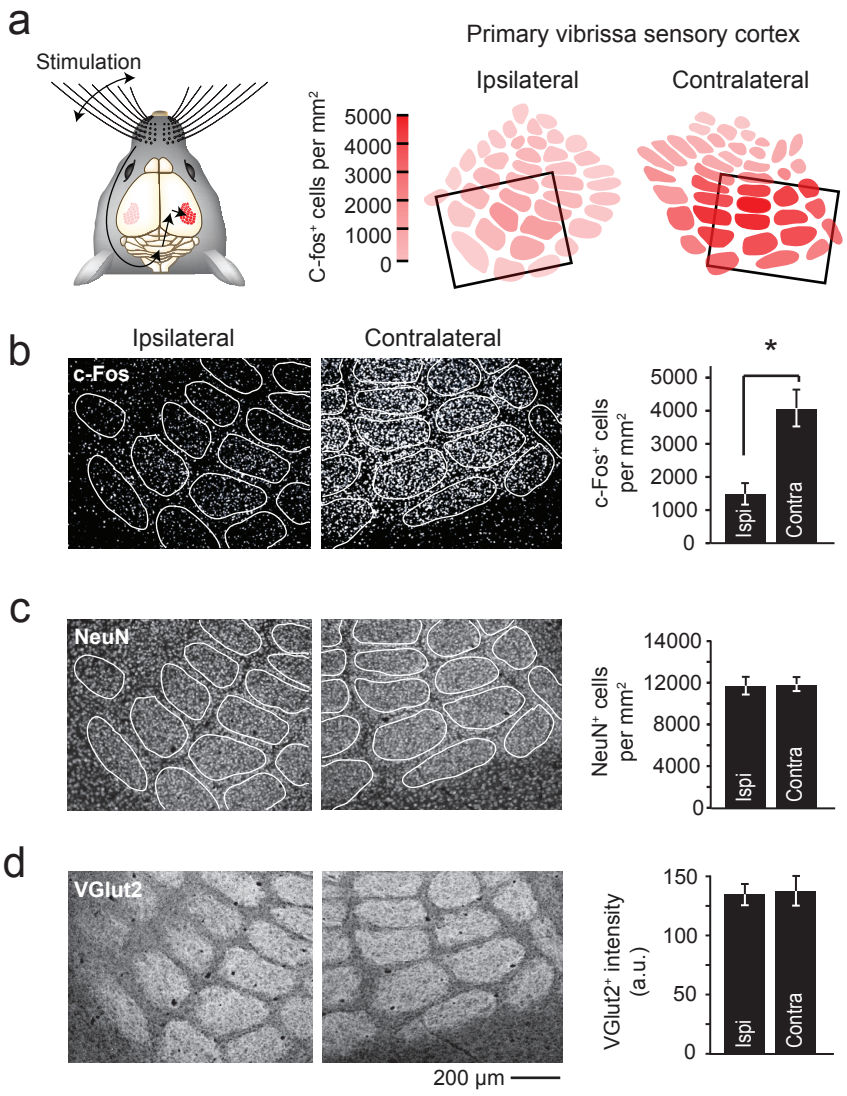

Supplementary Figure 2 (Summers ... Shih)

Supplemental Material for "Functional deficits induced by cortical microinfarcts" by Philipp M. Summers, David A. Hartmann, Edward S. Hui, Xingju Nie, Rachael L. Deardorff, Emilie T. McKinnon, Joseph A. Helpern, Jens H. Jensen and Andy Y. Shih

Supplementary Figure 3. Strategic induction of microinfarcts in the barrel cortex of the primary sensory system. Example of a microinfarct (yellow circle) induced at the edge of the barrel cortex. The barrels have been labeled with VGlut2 immunostaining and are visible at the depth of cortical layer 4. The approximate location of the perilesional region (between yellow and blue lines) is also shown. This encompasses the major rows B,C and D and columns 1, 2 and 3, where c-Fos assays and hemodynamic imaging was performed. Barrel C2 is labeled with an asterisk.

Layer 4 of Primary Barrel Cortex

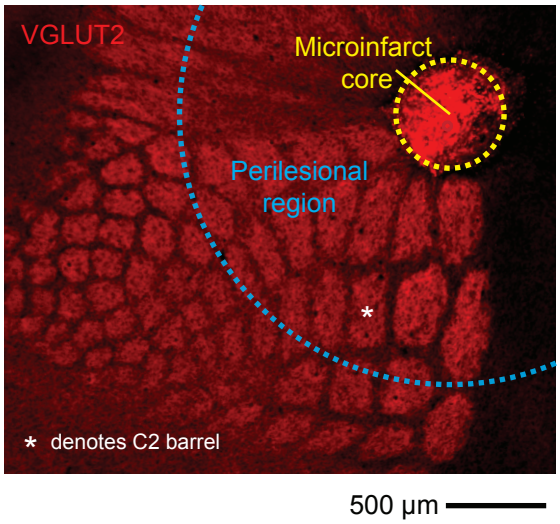

Supplementary Figure 3 (Summers ... Shih)

Supplemental Material for "Functional deficits induced by cortical microinfarcts" by Philipp M. Summers, David A. Hartmann, Edward S. Hui, Xingju Nie, Rachael L. Deardorff, Emilie T. McKinnon, Joseph A. Helpern, Jens H. Jensen and Andy Y. Shih

Supplementary Figure 4. Optimization of cell counting for using ITCN software. ITCN software (http://rsb.info.nih.gov/ij/plugins/itcn.html) was used to count the number of c-Fos and NeuN expressing cells in histological slices. An example for c-Fos assay analysis is shown here. **(a)** During initial optimization, we tested the effect of varying the cell diameter parameter between 10 to 20 pixels (0.98 pixels/μm). The cell counts obtained over 3 regions of interested were compared with hand-counted cell numbers from the same images. **(b)** A 15 pixel cell diameter was found to be optimal for the images collected in this study. Smaller cell diameter (5 or 10 pixels) inputs led to false positives, while larger cell diameters (20 pixels) under-estimated the number of cells.

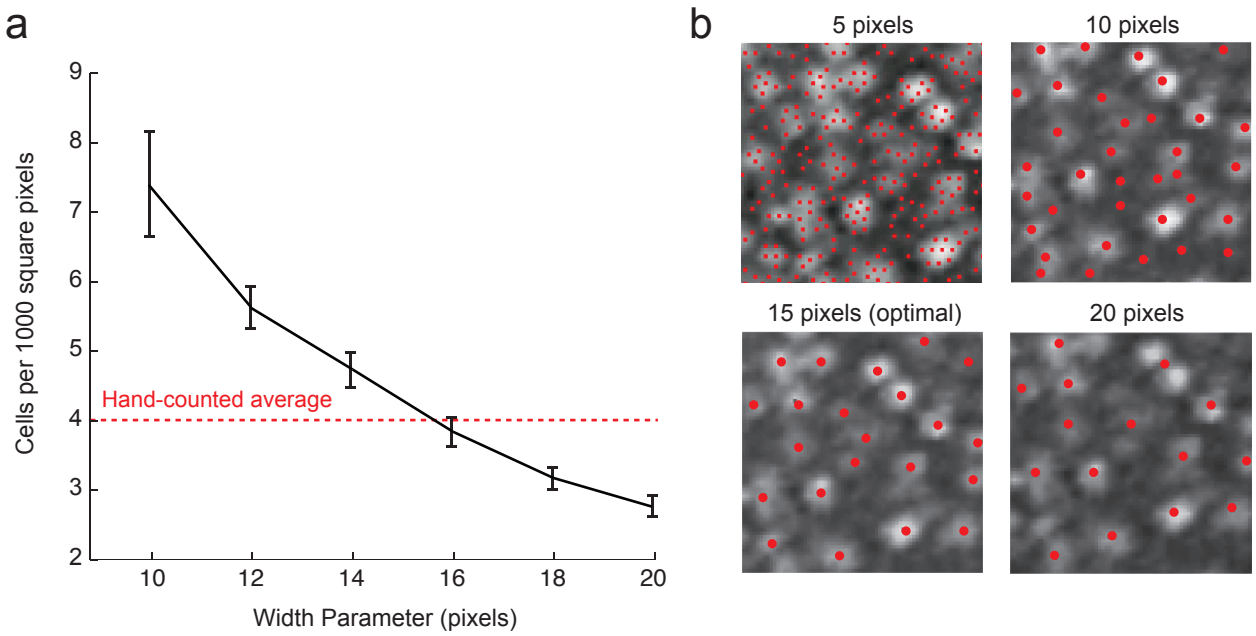

Supplementary Figure 4 (Summers ... Shih)

Supplemental Material for "Functional deficits induced by cortical microinfarcts" by Philipp M. Summers, David A. Hartmann, Edward S. Hui, Xingju Nie, Rachael L. Deardorff, Emilie T. McKinnon, Joseph A. Helpern, Jens H. Jensen and Andy Y. Shih

Supplementary Figure 5. MRI signals associated with evolution of microinfarct pathology. Longitudinal imaging of 2 microinfarcts (same animal as in **Figure 2a**), with additional imaging sequences including, T1, T2* (TE = 11 ms), and MD. Green circles in left column show location of on-target vessel occlusion. Yellow circle shows location of an off-target irradiation.

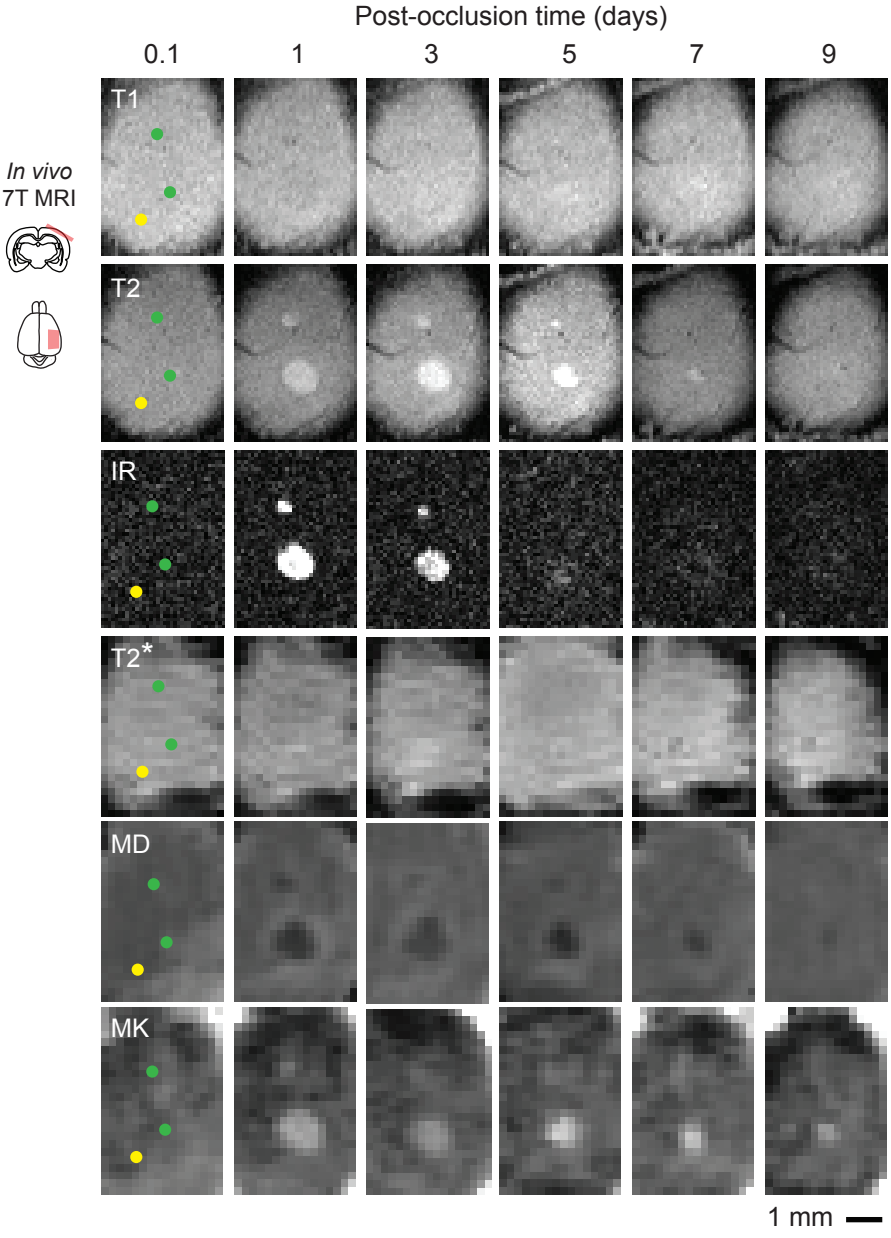

Supplementary Figure 5 (Summers ... Shih)

Supplemental Material for "Functional deficits induced by cortical microinfarcts" by Philipp M. Summers, David A. Hartmann, Edward S. Hui, Xingju Nie, Rachael L. Deardorff, Emilie T. McKinnon, Joseph A. Helpern, Jens H. Jensen and Andy Y. Shih

Supplementary Figure 6. Additional examples of microinfarcts imaged longitudinally with MRI. In both examples, green circles in left column show location of on-target vessel occlusion. With mouse 513b, top and middle lesion are venular microinfarcts, while the lower lesion is an arteriole microinfarct. With mouse 402, top medial lesion is a venular microinfarct, while the other two lesions are arteriole microinfarcts.

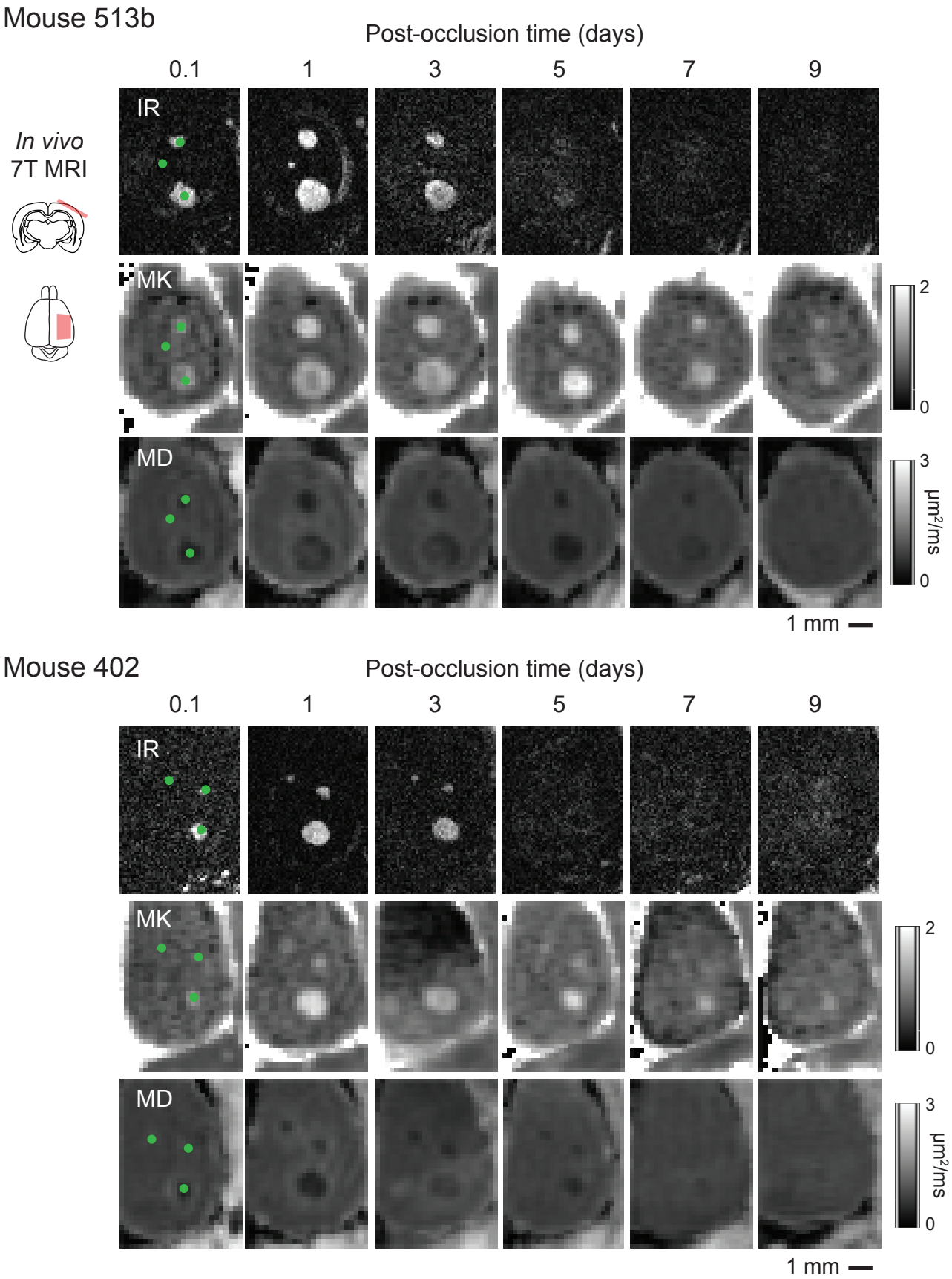

Supplementary Figure 6 (Summers ... Shih)

Supplemental Material for "Functional deficits induced by cortical microinfarcts" by Philipp M. Summers, David A. Hartmann, Edward S. Hui, Xingju Nie, Rachael L. Deardorff, Emilie T. McKinnon, Joseph A. Helpern, Jens H. Jensen and Andy Y. Shih

Supplementary Figure 7. Arteriole and venular microinfarcts evolve over a similar timescale. (a-c) Average area of microinfarct plotted as a function of post-occlusion time. Error bars show standard error of the mean. Venular microinfarcts (blue) were on average smaller compared to arteriole microinfarcts (red); data from n = 12 penetrating arteriole and n = 8 penetrating venule occlusions over 7 mice. This was because penetrating venules of lower red blood cell flux were targeted in order to reduce the likelihood of secondary effects on neighboring arterioles (Taylor *et al.*, JCBFM, 2016, 36(8):1357-73). **(d-f)** Microinfarct area normalized to peak area (1 or 3 days). Note that despite venular microinfarcts being smaller, the evolution of MRI signal change is comparable to arteriole microinfarcts. That is, the microinfarct area peaks at 1-3 days post-occlusion and then begins to decrease until visibility is lost by 9 days post-occlusion for DKI and 5-7 days post-occlusion for structural MRI sequences.

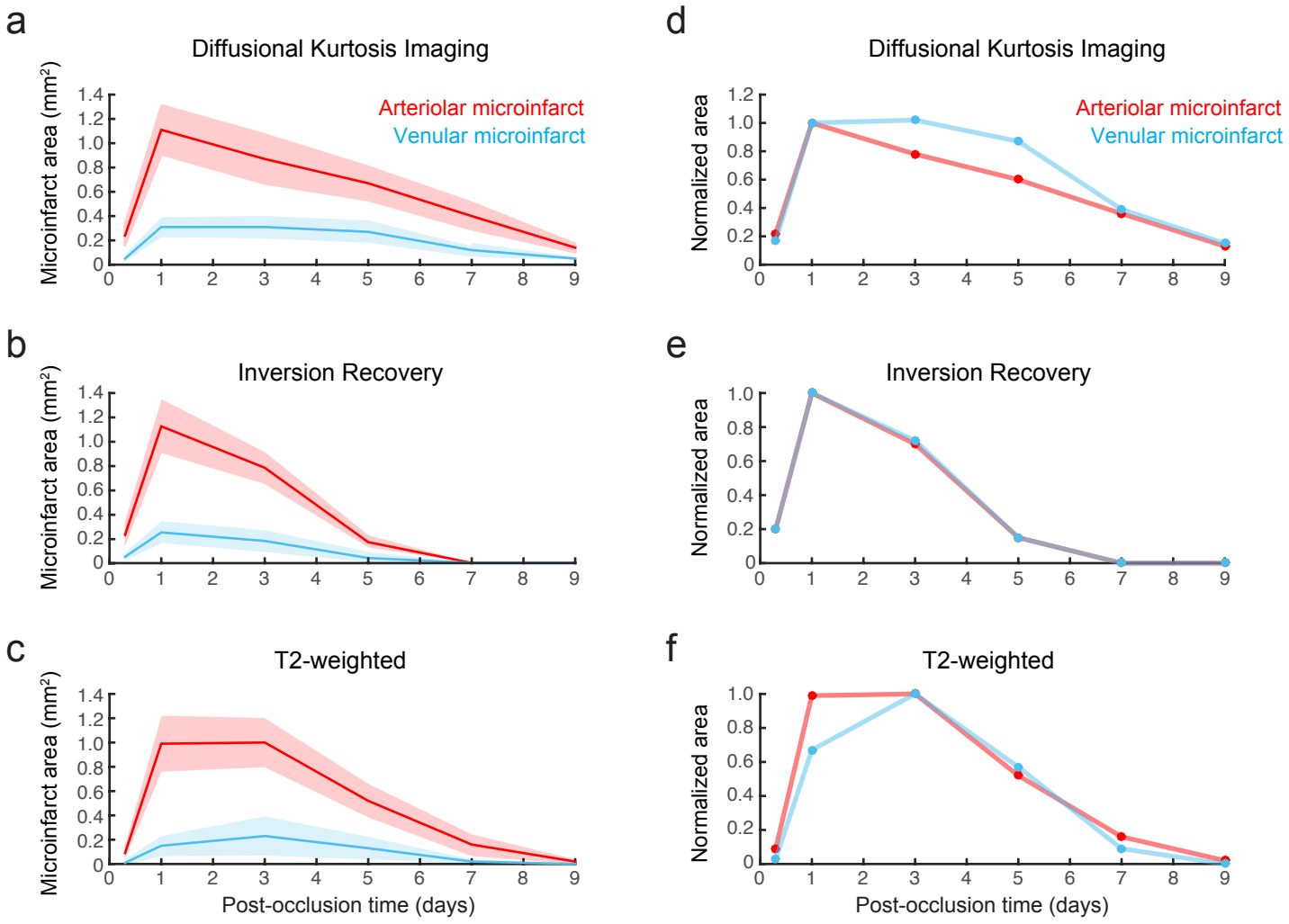

Supplementary Figure 7 (Summers ... Shih)

Supplemental Material for "Functional deficits induced by cortical microinfarcts" by Philipp M. Summers, David A. Hartmann, Edward S. Hui, Xingju Nie, Rachael L. Deardorff, Emilie T. McKinnon, Joseph A. Helpern, Jens H. Jensen and Andy Y. Shih

Supplementary Figure 8. Synaptophysin immunostaining is not affected in microinfarct perilesional tissues. (a) The microinfarct core (demarcated by yellow dashed line) can be observed in NeuN-stained tissues two days post-occlusion. NeuN immunostaining intensity was sampled from 11 regions of interest (white boxes). **(b)** Average intensity of NeuN staining (normalized to the intensity of a region several millimeters from the microinfarct) did not significantly change with distance from microinfarct border ($p = 0.9$ main effect; $F(10,22) = 0.2$; one-way ANOVA; $n = 3$ mice; 3 brain slices examined per mouse). Data is mean ± SEM. **(c)** Synaptophysin, a presynaptic marker, stained in the same slice shown in panel (a). The decrease in synaptophysin expression within barrels is well-documented under physiological conditions (Sehara *et al*. J. Neurosci, 2010, 30(8):3082-92). Average intensity of synaptophysin staining was calculated from the same regions of interest shown in panel (a). Staining was achieved with rabbit anti-synaptophysin antibody (ab32127; Abcam), followed by anti-rabbit Alexa 594 secondary antibody (A31632; ThermoFisher). **(d)** Average intensity of synaptophysin (normalized to the intensity of a region several millimeters from the microinfarct) did not significantly change with increasing distance from microinfarct border ($p = 0.9$ main effect; $F(10,22) = 0.1$; One-way ANOVA; $n = 3$ mice; 3 brain slices examined per mouse). Data is mean ± SEM.

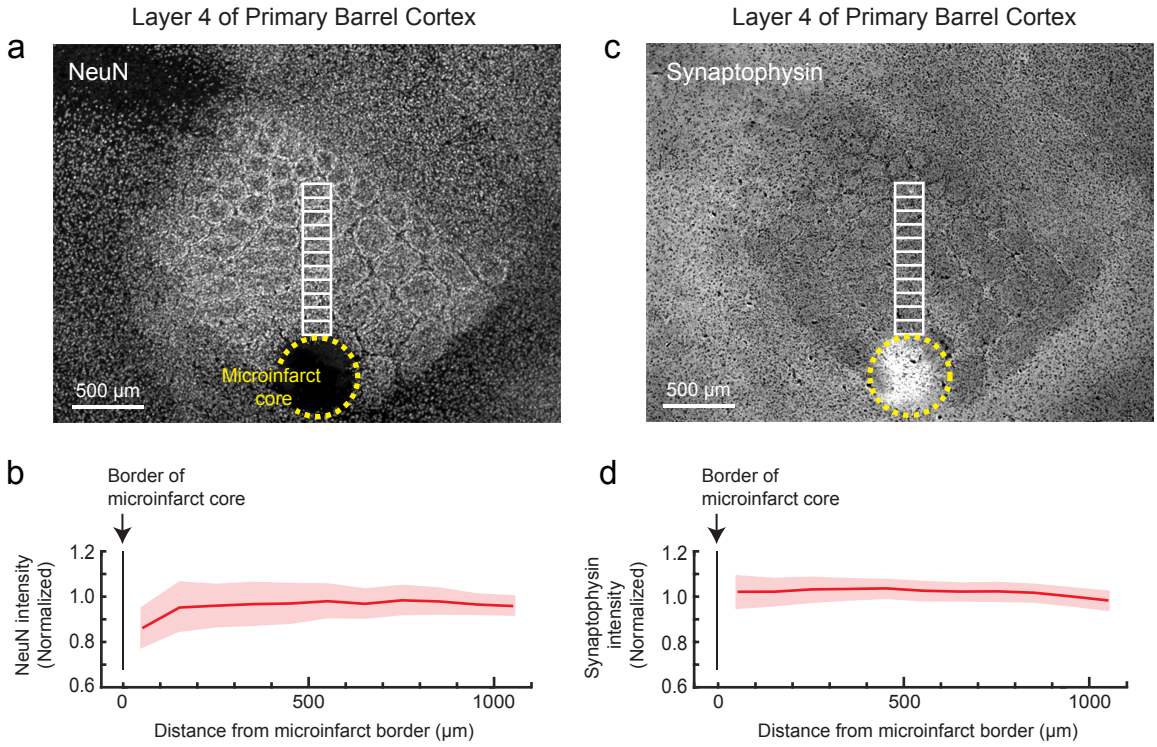

Supplementary Figure 8 (Summers ... Shih)

Supplemental Material for "Functional deficits induced by cortical microinfarcts" by Philipp M. Summers, David A. Hartmann, Edward S. Hui, Xingju Nie, Rachael L. Deardorff, Emilie T. McKinnon, Joseph A. Helpern, Jens H. Jensen and Andy Y. Shih

Supplementary Figure 9. Sensory-evoked hemodynamics during the hyperacute phase of microinfarct injury. (a) Mean change in pial arteriole diameter during vibrissal stimulation, plotted as a function of post-occlusion time (*$p < 0.05$ compared to pre-occlusion, one-way ANOVA with repeated measures followed by Tukey's *post test*; n = 28 arterioles over 3 mice with single arteriole microinfarcts). Data is mean ± SEM. **(b)** Sensory-evoked arteriole dilation pre-occlusion and at various times following penetrating arteriole occlusion. **(c-f)** Mean change in arteriole diameter plotted as a function of distance from the occluded penetrating arteriole. Responses from the same arterioles are re-plotted for 20, 60, 120 and 180 minutes post-occlusion imaging time points. Red lines correspond to second order polynomial regression fits of the data. A gray lines shows the approximate microinfarct core and perilesion boundary based on the ~ 200 μm average radius of the microinfarct core.

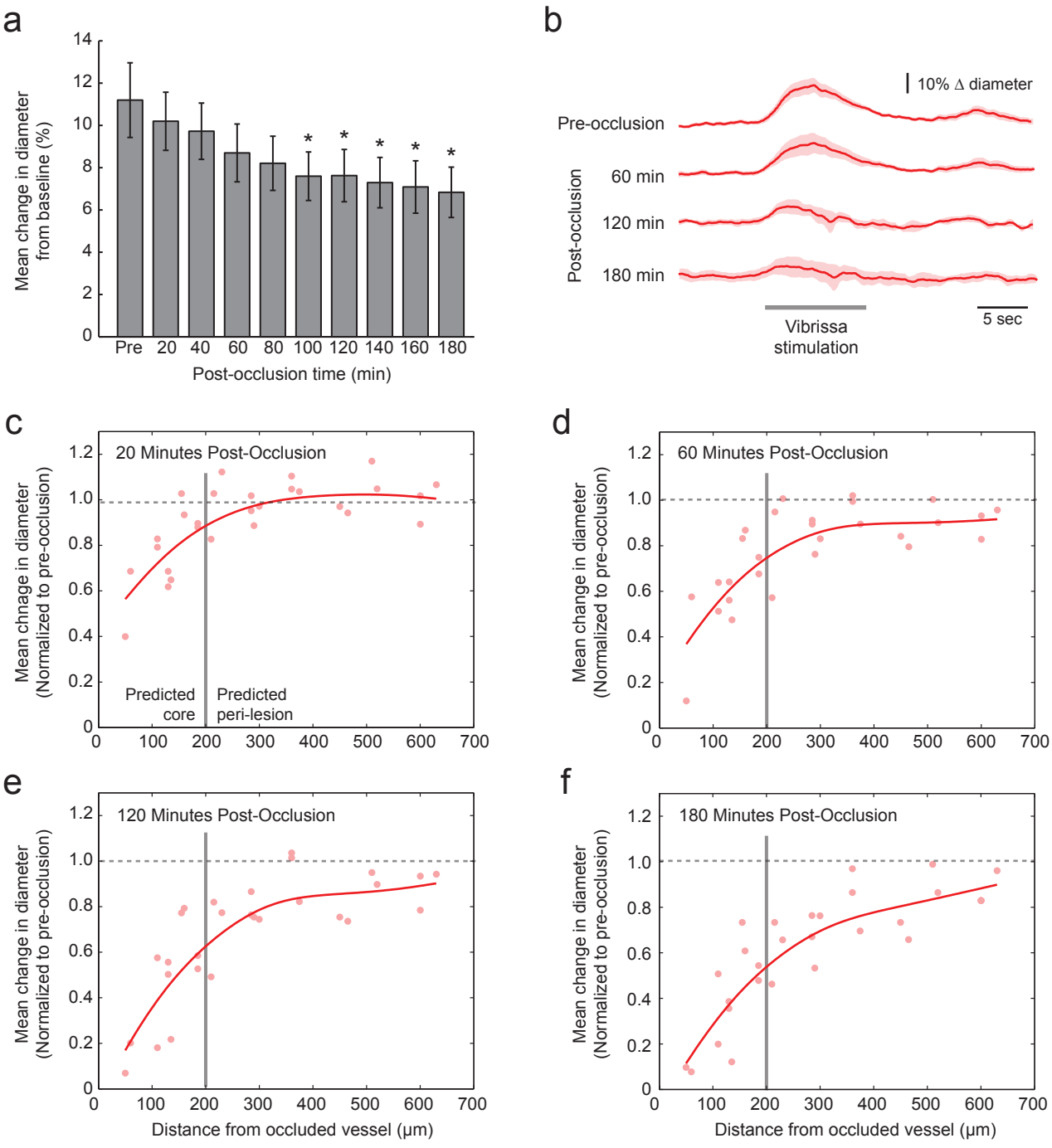

Supplementary Figure 9 (Summers ... Shih)

Supplemental Material for "Functional deficits induced by cortical microinfarcts" by Philipp M. Summers, David A. Hartmann, Edward S. Hui, Xingju Nie, Rachael L. Deardorff, Emilie T. McKinnon, Joseph A. Helpern, Jens H. Jensen and Andy Y. Shih

Supplementary Figure 10. Hemodynamic function after sham occlusion. Chronic imaging after sham occlusion (green laser irradiation of a penetrating arteriole, but no intravenous Rose Bengal) reveals stable sensory-evoked hemodynamic signals. No significant differences were detected between imaging timepoints ($p = 0.3$ main effect, $F(2.1, 68.3) = 1.22$, one-way ANOVA with repeated measures; $n = 33$ arterioles over 3 mice). Data = mean ± SEM.

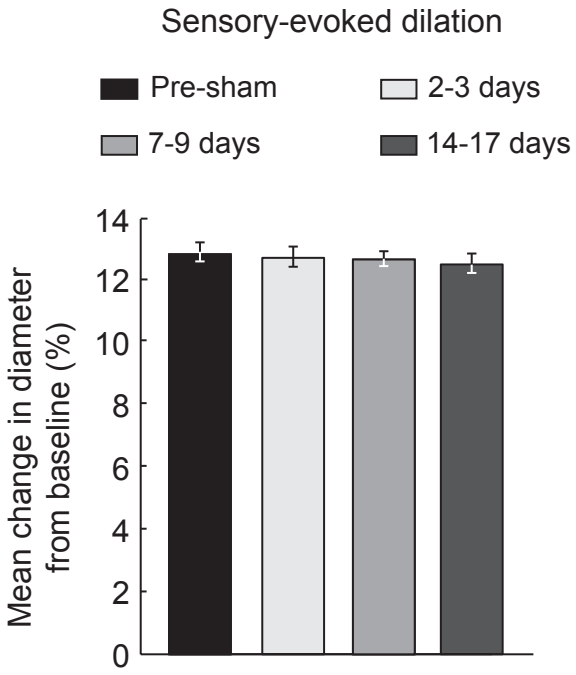

Supplementary Figure 10 (Summers ... Shih)

Supplemental Material for "Functional deficits induced by cortical microinfarcts" by Philipp M. Summers, David A. Hartmann, Edward S. Hui, Xingju Nie, Rachael L. Deardorff, Emilie T. McKinnon, Joseph A. Helpern, Jens H. Jensen and Andy Y. Shih

Supplementary Figure 11. Latency in onset of sensory-evoked arteriole dilation after microinfarct induction. (a) Latency to dilation for each arteriole (normalized to pre-occlusion values) plotted as a function of distance from the histologically verified microinfarct core border. The point of dilation onset is computed as when the arteriole diameter exceeds 2-times the standard deviation of the pre-stimulation baseline. **(b,c)** Equivalent plots of latency to dilation for data collected 7-9 days and 14-21 days post-occlusion. (n = 50, 36 and 24 arterioles over 6 mice for panels (a), (b) and (c), respectively).

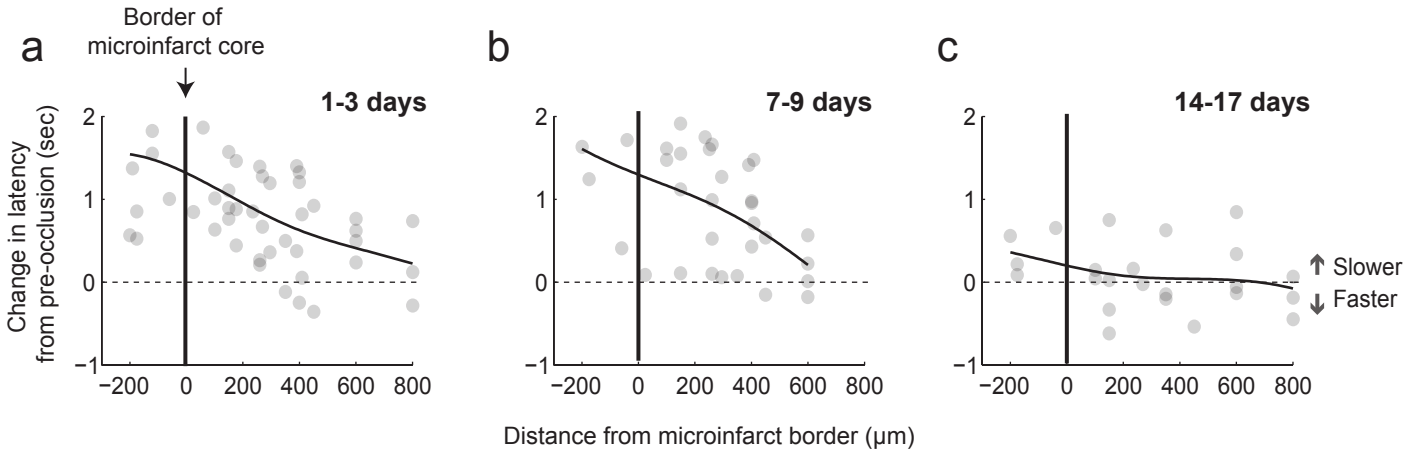

Supplementary Figure 11 (Summers ... Shih)

Supplemental Methods.

Synaptophysin immunohistochemistry. For synaptophysin studies, tissues were prepared as described for c-Fos. Immunostaining was performed with anti-NeuN from guinea pig host (ABN90P; 1:1000 dilution; Millipore) and synaptophysin from rabbit host (ab32127; 1:250 dilution; Abcam). Secondary antibodies consisted of anti-guinea pig Alexa 488 (A18776, 1:500 dilution, ThermoFisher) and anti-rabbit Alexa 594 (A11076; 1:1,000 dilution; ThermoFisher). Image J was used to quantify the mean fluorescence intensity of VGlut2 (**Fig. 4**), as well as NeuN and synaptophysin immunostains (**Supplementary Fig. 8**). Cell counts or intensity measurements were calculated from ROIs (100 x 200 μm) placed at increasing distances (100 μm intervals) from the microinfarct border.

Dendritic Spine Analysis. Penetrating arteriole occlusion was induced in Thy1-YFP H mice (Jackson Laboratories #003782) under guidance of intravenous cascade blue-dextran (10 kDa; D1976; ThermoFisher)(**Fig. 5**). Two days after occlusion, animals were perfusion-fixed and tissues were processed as described for c-Fos studies. Sections were immunostained with guinea pig NeuN primary antibody followed by and Alexa 594 secondary (see above). Wide-field confocal images of the microinfarct border were collected using an Olympus BX61 microscope with a UPLSAPO10x2 objective lens (0.345 pixels per μm lateral resolution, 1 μm Z step size). Individual somata and basal dendrites of layer II/II pyramidal neurons were identifiable at this low resolution. We then imaged at high-resolution, 28 neurons (n = 2 mice) spanning a range of distances from the microinfarct border. High-resolution imaging was performed with a UPLSAPO 60xO objective lens (8.8 pixels per μm lateral resolution, 0.5 μm Z step size), with laser and PMT parameters kept comparable for all cells. For analysis, images were presented in random order to an examiner blinded to the distance from the microinfarct border, who then Z projected and cropped dendrite segments (typically 10 per cell) in ImageJ. Counting of spines on dendritic segments was manually performed by two examiners also blind to the distance from the microinfarct border. Bland-Altman analysis on a shared data set showed good agreement between the two examiners' counts with equal inter-rater differences across the spectrum of spine densities (reproducibility coefficient 14 spines/100 μm segment, Pearson $R = 0.85$, $p < 0.0001$). Both examiners analyzed segments from all 28 cells so that any inter-examiner differences would be balanced within each cell. A total of 3584 spines along 13.1 mm of dendrite length was counted.

MRI scanning protocols. Images were acquired tangential to the surface of the cortex to provide a plane similar to that obtained with two-photon microscopy over the cranial window (Protocols 1, 3-6). One T2-weighted protocol collected images in the coronal orientation (Protocol 2).

1. T2-weighted (axial): Repetition time (TR) / echo time (TE) = 2500/33 ms, RARE Factor = 8, field of view (FOV) = 25.6 × 25.6 mm^2, matrix = 256 × 256, voxel dimension = 0.1 × 0.1 × 0.3 mm^3, number of slices = 20, number of signal averages = 4, scan time = 5 minutes 20 seconds.

2. T2-weighted (coronal): Same as Protocol 1 except for the following parameters: number of slices = 8, number of signal averages = 2, scan time = 2 minutes 40 seconds.

3. Inversion recovery (axial): TR/TE/inversion time = 5000/33/837 ms, FOV = 25.6 × 25.6 mm^2, matrix = 256 × 256, voxel dimension = 0.1 × 0.1 × 0.3 mm^3, number of slices = 8, number of signal averages = 2, scan time = 5 minutes 20 seconds.

4. T1-weighted (axial): TR/TE = 1300/9 ms, RARE Factor = 4, FOV = 25.6 × 25.6 mm^2, matrix = 256 × 256, voxel dimension: 0.1 × 0.1 × 0.3 mm^3, number of slices = 8, number of signal averages = 2, scan time = 2 minutes 5 seconds.

5. T2*-weighted (axial): TR/TE = 1500/(4, 11, 18, 25, 32, 39) ms, flip angle = 30°, FOV = 25.6 × 25.6 × 2.4 mm^3, matrix = 256 × 256 × 8, voxel dimension = 0.1 × 0.1 × 0.3 mm^3, number of signal averages = 1, scan time = 19 minutes 12 seconds.

6. Diffusional kurtosis imaging (axial): multi-shot diffusion-weighted echo planar imaging, number of shots = 4, b-value = [0, 1000, 2000] s/mm^2, diffusion-encoding directions = 64, δ/Δ = 5/18 ms, TR/TE = 3000/30.46 ms, FOV = 25.6 × 25.6 mm^2, matrix = 128 × 128, voxel dimension = 0.2 × 0.2 × 0.3 mm^3, number of slices = 8, bandwidth = 250 kHz, number of signal averages = 2, scan time = 59 minutes 12 seconds. For Data of **Fig. 8**, all imaging parameters were the same, except voxel dimension = 0.078 × 0.078 × 0.5 mm^3.